

Structural and new spectroscopic properties of neutral $[M(\text{dmit})_2]$ ($\text{dmit} = \text{C}_3\text{S}_5^{2-}$, 1,3-dithiole-2-thione-4,5-dithiolate) and $[M(\text{H}_2\text{timdt})_2]$ ($\text{H}_2\text{timdt} = \text{H}_2\text{C}_3\text{N}_2\text{S}_3^{1-}$, monoanion of imidazolidine-2,4,5-trithione) complexes within the density functional approach

Pina Romaniello · Francesco Lelej ·
Massimiliano Arca · Francesco A. Devillanova

Received: 12 September 2006 / Accepted: 13 November 2006 / Published online: 5 January 2007
© Springer-Verlag 2006

Abstract We give a detailed description of the structural, electronic and optical properties of the $[M(\text{dmit})_2]$ ($M = \text{Ni}, \text{Pd}, \text{Pt}$) neutral dithiolenes by calculating their geometries, their bonding energies, their vibrational spectra, their ground and excited electronic states within the density functional approach. The dominant relativistic effects are treated by using the zeroth-order regular approximation. We compare their properties with those of the similar $[M(\text{H}_2\text{timdt})_2]$ ($M = \text{Ni}, \text{Pd}, \text{Pt}$) series of dithiolenes and we find, in particular, that the LUMOs in the $[M(\text{dmit})_2]$ compounds lay at energy very close to those of the HOMOs in the corresponding $[M(\text{H}_2\text{timdt})_2]$ compounds, which indicates the mixed-ligand complexes as possible non-linear optical materials. The analysis of the UV–vis–NIR spectrum of the $[\text{Ni}(\text{dmit})_2]$ complex shows that the intense NIR absorption is redshifted with respect to that in $[\text{Ni}(\text{H}_2\text{timdt})_2]$, which may candidate this compound as dyes for Q-switching and/or mode locking the Nd:YAG and Nd:YLF lasers.

Keywords d^8 Transition-metal ions · Density functional calculations · Dithiolenes · Scalar relativistic effects · ZORA · TD-DFT

1 Introduction

The general class of metal-dithiolenes represents a very important set of coordination compounds because of their unique properties such as optical nonlinearities, electrical conduction, the ability to exist in several oxidation states all connected through fully reversible redox steps, and in particular an intense absorption in the NIR region of the spectrum [1–4]. The dithiolenes derived from the dmit ligand ($\text{dmit} = \text{C}_3\text{S}_5^{2-}$, 1,3-dithiole-2-thione-4,5-dithiolate) together with the group ten transition metal ions are the most known due to their low temperature electrical superconducting properties [5–12]. Recent reviews on this class of compounds can be found in Refs. [13–17]. Whereas several studies have been performed on the anionic forms of these complexes, the literature lacks an in-depth investigation of the neutral $[M(\text{dmit})_2]$ ($M = \text{Ni}, \text{Pd}, \text{Pt}$) series. In order to get a deeper insight into their ground-state electronic structure and, in particular, in the optical properties of these neutral complexes, the ground-state geometry, the vibrational frequencies and the electronic excitation energies have been calculated by using the DFT and TD-DFT approaches [18–20]. Relativistic effects [21, 22] have been considered at scalar level by using the method of zeroth-order regular approximation (ZORA) [23–25]. Only the neutral Ni complex has been isolated and characterised until now [13–16]. However, since a very good agreement is found between the calculated scalar relativistic geometries and the available experimental data [26–29] for the similar $[M(\text{H}_2\text{timdt})_2]$ ($\text{H}_2\text{timdt} = \text{H}_2\text{C}_3\text{N}_2\text{S}_3^{1-}$, monoanion of imidazolidine-2,4,5-trithione) class of model complexes, present calculations are expected to predict very well the geometry of the $[M(\text{dmit})_2]$ ($M = \text{Pd}, \text{Pt}$) complexes. We

P. Romaniello · F. Lelej (✉)
LAMI Dipartimento di Chimica and LASCAMM—INSTM
Sezione Basilicata, Università della Basilicata,
Via N. Sauro, 85100 Potenza, Italy
e-mail: lelej@unibas.it

M. Arca · F. A. Devillanova
Dipartimento di Chimica Inorganica ed Analitica,
S.S. 554 Bivio per Sestu, 09042 Monserrato-Cagliari, Italy

further characterise these complexes by calculating their vibrational frequencies and by assigning the experimental Raman and IR spectra present in the literature for the neutral $[\text{Ni}(\text{dmit})_2]$ complex. We then give a detailed description of the UV–vis–NIR spectrum of the neutral $[\text{Ni}(\text{dmit})_2]$ complex. Unfortunately, the literature lacks the experimental spectrum for the neutral form. However, we have estimated the NIR absorption λ_{max} by decomposing with Gaussian curves the recorded spectrum containing both the monoanionic and neutral forms in solution. This information, together with the level of agreement found between calculated and measured spectrum of the $[\text{Ni}(\text{H}_2\text{timdt})_2]$ model complex, gives a reasonable confidence to the description of the $[\text{Ni}(\text{dmit})_2]$ spectrum within the used theoretical approach.

2 Theoretical and experimental procedures

2.1 Calculations

Density functional theory is a successful formalism firmly based on the two theorems formulated and proved by Hohenberg and Kohn in 1964 [18]. In 1984, Runge and Gross extended the original derivation for ground state to the time dependent case (TD-DFT). The time-dependent density-functional response theory (TD-DFRT) was later formulated and offers a formally exact theory for calculating excitation energies [19,20,30]. Our current work involves the adiabatic approximation and the use of appropriate exchange-correlation (xc) functionals [31], i.e., the generalised gradient approximated functionals (GGAs) by Becke [32] for the exchange and Perdew [33] for the correlation parts (BP), the Becke exchange with the correlation functional developed by Lee et al. [34], in a hybrid HF/DFT scheme (B3LYP) [35], the PBE (by Perdew, Burke and Ernzerhof) and its variant PBE0 GGA model [36,37], the asymptotically correct potential LB94 proposed by Van Leeuwen and Baerends [38], and the new SAOP (statistical average of orbital potentials) [39,40]. The calculations have been performed by using the Gaussian98 A.11 package [41] and the ADF 2000 package [42]. The latter allows also to consider the dominant scalar relativistic effects by using the ZORA. All ground-state molecular geometries used in our calculations have been optimised at scalar relativistic ZORA level assuming the D_{2h} symmetry. We have used the BP approximation for the ground-state xc-functional and the ADF/ZORA V basis set [43], which is an optimised valence triple- ζ STO basis set with two polarisation functions, for main element atoms, and the ADF/ZORA IV basis set, which is

a triple- ζ nd , $(n+1)$ s basis with one $(n+1)$ p function, for the metals. The cores (C, N: $1s$; S, Ni: $1s-2p$; Pd: $1s-3d$; Pt: $1s-4d$) have been kept frozen. To show the relevance of the relativistic effects, we have also performed nonrelativistic geometry optimisations. Scalar relativistic ZORA vibrational frequencies have been calculated by using relativistically optimised geometries. Following a recent study on the $[\text{M}(\text{H}_2\text{timdt})_2]$ ($\text{M} = \text{Ni}, \text{Pd}, \text{Pt}$) [26], vertical excitation energies have been evaluated in the same basis set used in the geometry optimisation for the calculation with the ADF package. The 6-31g* basis set has been used for the calculations with the Gaussian98 package.

2.2 Experiments

$[\text{Bu}_4\text{N}]_2[\text{Ni}(\text{dmit})_2]$ and $[\text{Ni}(\text{Et}_2\text{timdt})_2]$ have been obtained and characterised as previously reported [1,26,44,45]. UV–vis–NIR spectra (250–2,000 nm) were recorded with a cell of a 1 cm optical path, on a Varian Cary 5 spectrophotometer at 20°C in a thermostatted compartment. Infrared spectra were recorded on a Bruker IFS55 spectrometer at room temperature, purging the sample cell with a flow of dried air. Polythene pellets with a Mylar beam-splitter and polythene windows ($500\text{--}50\text{ cm}^{-1}$, resolution 2 cm^{-1}) and KBr pellets with a KBr beam-splitter and KBr windows ($4,000\text{--}400\text{ cm}^{-1}$, resolution 4 cm^{-1}) were used. FT-Raman spectra were recorded with a resolution of 4 cm^{-1} on a Bruker RFS100 FT-Raman spectrometer, fitted with an In–Ga–As detector (room temperature) operating with a Nd–YAG laser (excitation wavelength 1,064 nm), with a 180° scattering geometry. Spectra decompositions were performed with the Specpeak 2.0 software [46] in the spectral range between 800 and $1,500\text{ cm}^{-1}$. The spectra recorded with both the monoreduced and the neutral form of $[\text{Ni}(\text{dmit})_2]$ present in solution were fitted with four main Gaussian curves (positioned at 859.71, 1001.64, 1150.96 and 1334.82 nm; half-bandwidths 100.94, 128.80, 214.25, and 174.67 nm, respectively) and with a further one (at 1453.34 nm; half-bandwidth 251.75 nm) introduced in order to account for the baseline.

3 Results

3.1 Geometries and electronic structures

Nonrelativistic and scalar relativistic density functional geometry optimisations have been performed for the $[\text{M}(\text{dmit})_2]$ dithiolenes [$\text{M} = \text{Ni}$, **1**; Pd, **2**; Pt, **3**] (Fig. 1). Since complexes **2** and **3** have not been isolated so far,

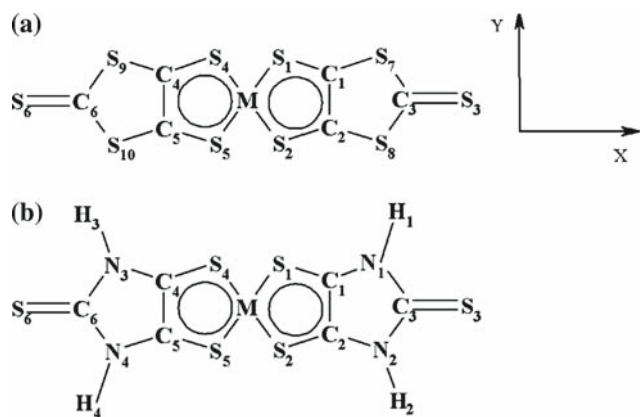


Fig. 1 $[M(\text{dmit})_2]$ neutral dithiolenes ($M = \text{Ni}$, **1**; Pd , **2**; Pt , **3**; $\text{dmit} = \text{C}_3\text{S}_5^{2-}$, 1,3-dithiole-2-thione-4,5-dithiolate) (a) and $[M(\text{H}_2\text{timdt})_2]$ neutral model dithiolenes ($M = \text{Ni}$, **1'**; Pd , **2'**; Pt , **3'**; $\text{H}_2\text{timdt} =$ monoanion of imidazolidine-2,4,5-trithione) (b)

we do not have experimental data for a direct comparison with our calculations. However, the relativistic Ni–S bond length is in excellent agreement with the measured one, as it becomes clear in Table 1 [6]. Furthermore, previous calculations performed on $[M(\text{H}_2\text{timdt})_2]$ ($M = \text{Ni}$, **1'**; Pd , **2'**; Pt , **3'**) series [26] (Fig. 1) have shown that relativistic corrections are essential in the correct description of the order in the metal–sulphur bond distances, which is $\text{Pd-S} \geq \text{Pt-S} > \text{Ni-S}$. These results suggest that also the geometry of the $[\text{Pd}(\text{dmit})_2]$ and $[\text{Pt}(\text{dmit})_2]$ complexes should be well described by the relativistic calculations. Using the relativistic geometry for the three complexes, the scalar relativistic molecular orbital energies have been computed (Fig. 2). As for the $[M(\text{H}_2\text{timdt})_2]$ complexes, all compounds show the ground state belonging to the A_g representation, the HOMO and the LUMO being the $5b_{1u}$ and the $5b_{2g}$ MOs (Fig. 3), respectively, considering the model molecule laying in the xy plane. The computed LUMOs of the $[M(\text{dmit})_2]$ complexes have energies (Fig. 4) more negative than those of the corresponding $[M(\text{H}_2\text{timdt})_2]$ complexes, in agreement with the experimental evidence that the former are much more reducible than the latter and that the anionic forms are more stable than the

neutral ones [1]. The HOMO–LUMO energy gap shows a minimum for complex **2**, as in the case of the $[M(\text{H}_2\text{timdt})_2]$ series. Furthermore, the complexes deriving by the dmit ligand show a larger gap than that of the corresponding complexes deriving by the H_2timdt ligand. It is noteworthy that LUMOs of the $[M(\text{dmit})_2]$ series lay at energy very close to those of the corresponding HOMOs of the $[M(\text{H}_2\text{timdt})_2]$ one. In particular, the $[\text{Pd}(\text{dmit})_2]$ complex has the LUMO lying at 5.186 eV and the $[\text{Pd}(\text{H}_2\text{timdt})_2]$ has the HOMO at 5.165 eV. This is a very interesting result for possible applications of the mixed-ligand complexes as non-linear optical material, in particular for the second-order response [27]. In order to analyse the interactions between the two ligands and the metal ion M^{2+} ($M = \text{Ni}$, Pd , Pt), we have used the fragment analysis proposed by Ziegler and Rauk [47,48]. The interaction energy (ΔE_{int}) is split up in two physically meaningful terms [49]:

$$\Delta E_{\text{int}} = \Delta E^0 + \Delta E_{oi}$$

Here, ΔE^0 is known as the steric repulsion energy and consists of two components: the classical electrostatic interaction (ΔE_{elstat}) between the unperturbed charge distributions of the interacting fragments, usually attractive, and the so-called Pauli repulsion (ΔE_{Pauli}), essentially due to the Pauli principle. The ΔE_{oi} term takes into account the attractive orbital interactions. The analysis of the bonding energy in terms of the bivalent metal M^{2+} [$M, d_{x^2-y^2}^2, d_{z^2}^2, d_{xy}^0, d_{xz}^2, d_{yz}^2, (n+1)s^0$] and the two dmit ligands considered as a single biantionic fragment (L^{2-}) shows a very strong interaction between the metal and the ligand, as found also for the $[M(\text{H}_2\text{timdt})_2]$ complexes (−35.25, −34.36 and −35.89 eV for Ni, Pd and Pt, respectively). However the metal has the tendency to interact more strongly with the H_2timdt than with the dmit ligand, in particular in the $[\text{Ni}(\text{H}_2\text{timdt})_2]$ complex the bonding energy is about 0.5 eV more negative than in the $[\text{Ni}(\text{dmit})_2]$ one. The mentioned trend is due to the steric term, that in the $[M(\text{dmit})_2]$ series is about 1.5 eV less negative than that computed for the $[M(\text{H}_2\text{timdt})_2]$ series. Thus, in spite of the larger orbi-

Table 1 Theoretical M–S bond lengths (Å) and S–M–S bond angles (deg) for the model compounds 1, 2 and 3 compared to the experimental data reported for the $[\text{Ni}(\text{dmit})_2]$ complex^a

Method	1		2		3	
	Ni–S	S–Ni–S	Pd–S	S–Pd–S	Pt–S	S–Pt–S
NR DFT	2.168	92.84	2.331	88.99	2.391	87.36
(SR) ZORA	2.158	93.07	2.303	89.60	2.298	89.23
Exp ^a	2.146(7)	92.70(5)	–	–	–	–

^a Taken from [4]. The $[\text{Pd}(\text{dmit})_2]$ and the $[\text{Pt}(\text{dmit})_2]$ neutral dithiolenes have not been isolated and characterised so far

Fig. 2 Orbital interaction diagram for compounds **1** and **1'** in terms of the neutral metal M^0 and two dmit and H_2timdt ligands, respectively, considered as a single neutral fragment

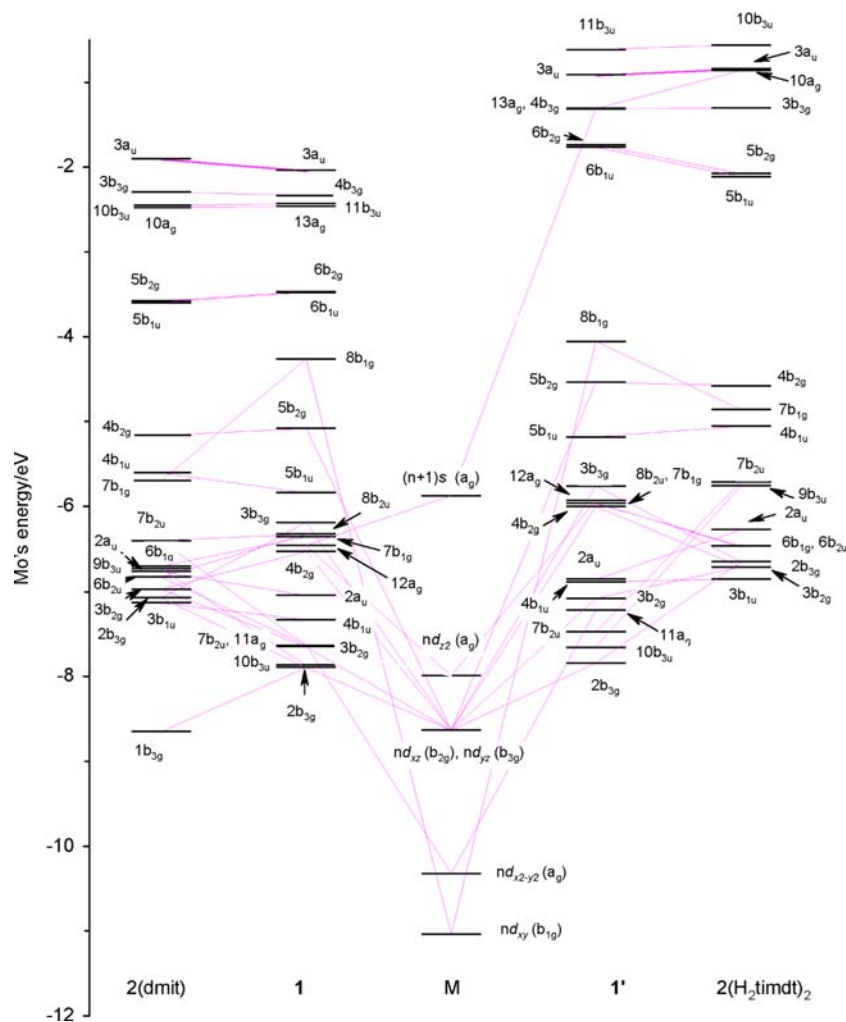
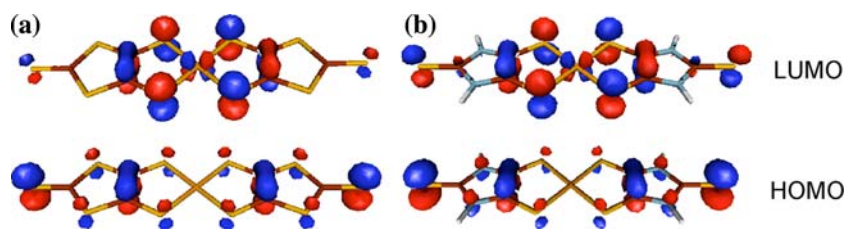


Fig. 3 Sketches of the HOMO and the LUMO for $[Ni(dmit)_2]$ (a) and $[Ni(H_2timdt)_2]$ (b) complexes



tal contribution with respect to the $[M(H_2timdt)_2]$ series, the larger Pauli repulsion and smaller electrostatic interaction found in the $[M(dmit)_2]$ complexes weaken their metal–ligand bonding (Fig. 5).

3.2 Vibrational spectrum

In order to provide a further understanding of the nature of $[M(dmit)_2]$ complexes, a systematic study of the vibrational spectrum has been performed. The experimental Raman and IR spectra with the relative assignment have been already reported in the literature

for the complex **1** [50]. However, there are no experimental data for the spectra of the Pd- and Pt-complexes and no one, to the best of our knowledge, has attempted a theoretical normal-mode calculation for these neutral complexes. Vibrational wave numbers of all the infrared active b_{1u} , b_{2u} and b_{3u} modes, the Raman active a_g and some b_{1g} modes, useful for the experimental Raman spectrum assignment, calculated for the $[M(dmit)_2]$ ($M = Ni, Pd, Pt$) neutral series are reported in Table 2 together with the experimental vibrational wave numbers of the compound **1**. Our calculations present some differences with respect to

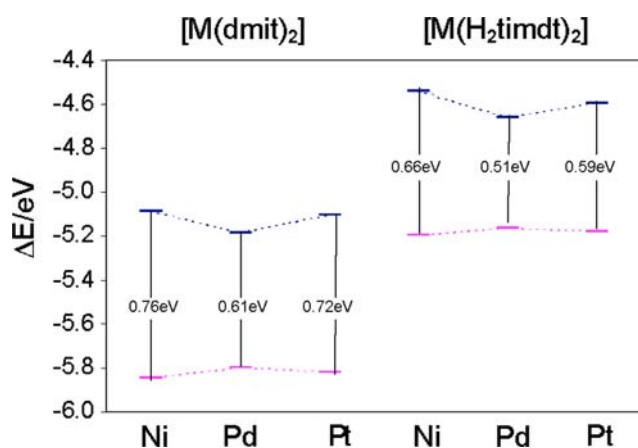


Fig. 4 HOMO–LUMO energy gap (eV) for $[M(\text{dmit})_2]$ and $[M(\text{H}_2\text{timdt})_2]$ ($M = \text{Ni}, \text{Pd}, \text{Pt}$) complexes

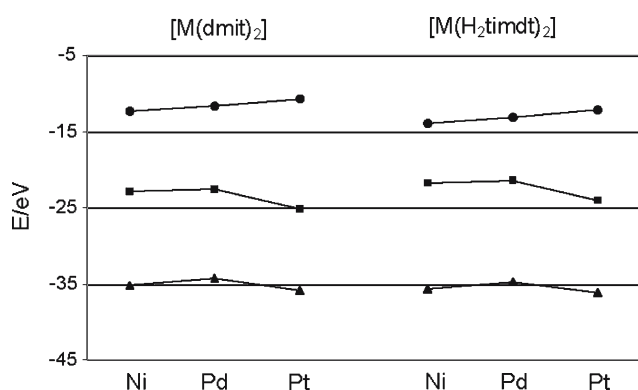


Fig. 5 Scalar relativistic steric interaction (ΔE^0 filled circle) and orbital interaction (ΔE_{oi} filled square) contributions to the bonding energy ($\Delta E^0 + \Delta E_{oi}$ filled triangle) for $[M(\text{dmit})_2]$ and $[M(\text{H}_2\text{timdt})_2]$ complexes

previous assignments of the vibrational spectrum recorded for the $[\text{Ni}(\text{dmit})_2]$ neutral complex. In the Raman spectrum, the band located at 496 cm^{-1} , previously attributed to the in-phase C=C and C–S stretching mode of the $\text{S}_2\text{C}=\text{CS}_2$ fragments [50], is originated from the a_g mode at 486 cm^{-1} , mainly involving the C–S–C bending of the *endocyclic* ring. Besides, in the previous assignment only the frequencies of a_g modes have been considered for the assignment of the Raman spectrum, whereas according to our calculations the two lowest frequency bands at 140 and 343 cm^{-1} could be also originated from the two b_{1g} modes at 142 and 338 cm^{-1} , respectively. We have found also a different assignment for the bands of the IR spectrum located at 328 and 485 cm^{-1} , previously attributed to the Ni–S stretching modes [51]. Indeed, according to our calculations, these two bands are originated from b_{3u} modes involving mainly the C=S stretching and the S–Ni–S bending, respectively. Besides, the medium intensive band at $1,088\text{ cm}^{-1}$, previously attrib-

uted to a C=S stretching, is not found in our calculations. The vibrational spectrum of the compounds **2** and **3** have been also calculated. Unlike the complex **1**, another medium intensive IR band located at 484 cm^{-1} (with intensity 37.9 km mol^{-1}) and at 362 cm^{-1} (with intensity 36.8 km mol^{-1}) for Pd- and Pt-complexes, respectively, might be observed. In order to understand the effect of the sulphur atoms of the *endocyclic* ring on the vibrational spectrum, we have compared the vibrational spectra of the $[\text{Ni}(\text{RR}'\text{timdt})_2]$ and $[\text{Ni}(\text{dmit})_2]$ complexes. A recent computational study on the $[\text{Ni}(\text{H}_2\text{timdt})_2]$ model complex [26] has suggested a possible assignment of the experimental vibrational bands falling in the region ranging between 50 and 500 cm^{-1} for several $[\text{Ni}(\text{RR}'\text{timdt})_2]$ compounds. The far-IR spectra show two main bands: the most intense one falls at $435(2)$ (average value) cm^{-1} , originated from the b_{3u} bending mode at 430 cm^{-1} in the relativistic ZORA calculations, and the latter falls at $380(2)\text{ cm}^{-1}$, attributed to the b_{3u} stretching mode (M–S) at 367 cm^{-1} . The Raman spectra show only two very intense bands at $330(4)$ and $434(1)\text{ cm}^{-1}$, deriving from the a_g stretching mode (M–S) at 332 cm^{-1} and from the b_{1g} bending mode at 423 cm^{-1} or the a_g bending mode at 429 cm^{-1} , respectively. In the case of the $[\text{Ni}(\text{dmit})_2]$ complex, the b_{3u} bending mode and the b_{3u} stretching mode responsible for the two bands in the $[\text{Ni}(\text{H}_2\text{timdt})_2]$ FIR spectrum, fall at 478 cm^{-1} with a medium intensity (65.7 km mol^{-1}) and at 401 cm^{-1} with a very low intensity (6.1 km mol^{-1}), respectively. The latter is not important for the FIR spectrum of the $[\text{Ni}(\text{dmit})_2]$ complex, for which the second experimental medium intensive band is attributed to the b_{3u} bending mode located at 333 cm^{-1} with high intensity (95.1 km mol^{-1}). Our calculations indicate that the vibrational modes responsible for the two intense Raman bands in the case of $[\text{Ni}(\text{H}_2\text{timdt})_2]$ complex fall at 359 cm^{-1} (the a_g stretching mode) and at 341 cm^{-1} (the a_g bending mode) or at 338 cm^{-1} (the b_{1g} bending mode) in the case of the $[\text{Ni}(\text{dmit})_2]$ complex. It is noteworthy that the nature of the lowest frequency Raman band changes passing from compound **1'** to **1**.

3.3 Electronic spectra of the $[\text{Ni}(\text{H}_2\text{timdt})_2]$ and $[\text{Ni}(\text{dmit})_2]$ complexes

As mentioned, the neutral $[\text{Ni}(\text{dmit})_2]$ complex is the only one of the series $[M(\text{dmit})_2]$ ($M = \text{Ni}, \text{Pd}, \text{Pt}$) to have been isolated and characterised via X-ray diffraction. However, its UV–vis–NIR spectrum has not been published yet, to the best of our knowledge. This lack of data may be attributed to the instability of the neutral form of $[\text{Ni}(\text{dmit})_2]$ in solution. Nevertheless, some information regarding the NIR absorption can be

Table 2 Scalar relativistic vibrational wave numbers (cm^{-1} ; IR relative intensities in parentheses in km mol^{-1}) calculated for complexes 1, 2 and 3 compared to the experimental IR and Raman spectra (cm^{-1}) of the $[\text{Ni}(\text{dmit})_2]$ neutral dithiolenes reported in Ref. [47]

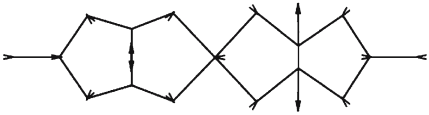
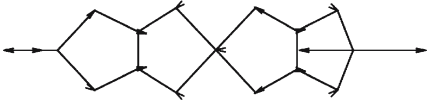
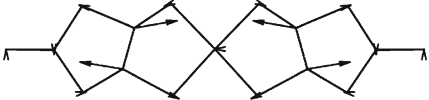




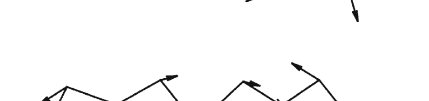
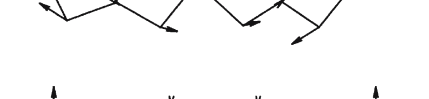
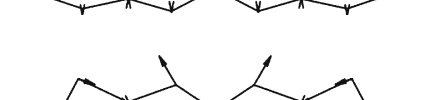
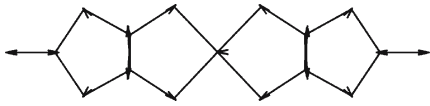
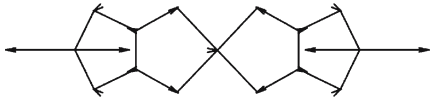
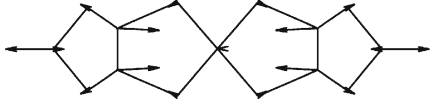
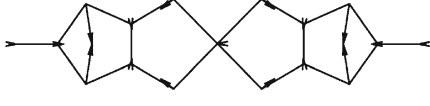
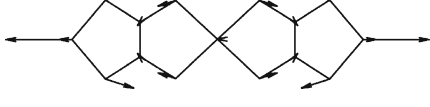

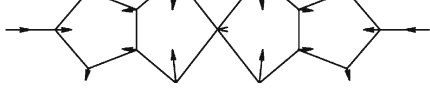
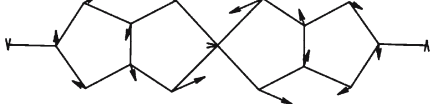
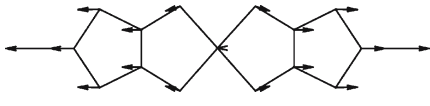
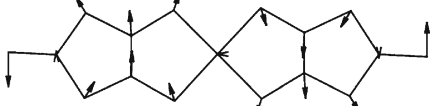
Mode	Mode description	Exp. $\bar{\nu}$ [$\text{Ni}(\text{dmit})_2$]	Calcd. $\bar{\nu}$		
			1	2	3
IR		1,260 (s)	1,277 (1327.9)	1,264 (1553.9)	1,277 (1551.4)
	–	1,088 (m)	–	–	–
		1,064 (s)	1,061 (802.1)	1,071 (814.6)	1,039 (790.7)
		–	1,022 (0.9)	1,012 (0.05)	1,021 (0.1)
		890 (m)	917 (45.7)	901 (39.9)	909 (40.3)
		–	840 (2.0)	844 (1.4)	847 (0.8)
		–	744 (26.7)	748 (26.8)	750 (31.1)
		–	487 (7.2)	484 (37.9)	484 (12.4)
		485 (m)	478 (65.7)	478 (31.0)	474 (46.3)
		–	431 (10.7)	431 (10.4)	429 (11)
		–	427 (0.6)	399 (1.9)	403 (1.7)

Table 2 continued

Mode	Mode description	Exp. $\bar{\nu}$ [Ni(dmit) ₂]	Calcd. $\bar{\nu}$		
			1	2	3
b _{3u}		–	402 (6.1)	357 (13.3)	362 (36.8)
b _{2u}		–	394 (2.1)	375 (0.8)	376 (0.5)
b _{3u}		328 (m)	333 (95.1)	324 (96.8)	355 (84.7)
b _{2u}		–	282 (0.7)	270 (0.9)	263 (0.7)
b _{1u}		–	280 (3.0)	282 (2.9)	286 (3.3)
b _{3u}		–	263 (0.2)	231 (0.2)	209 (0.06)
b _{1u}		–	218 (0.02)	180 (0.001)	174 (0.2)
b _{2u}		–	179 (0.4)	169 (0.3)	160 (0.2)
b _{1u}		–	79 (1.5)	77 (1.6)	79 (1.8)
b _{2u}		–	53 (0.001)	54 (0.003)	32 (0.001)
b _{1u}		–	9 (0.1)	5 (0.07)	12 (0.1)

Table 2 continued

Mode	Mode description	Exp. $\bar{\nu}$ [Ni(dmit) ₂]	Calcd. $\bar{\nu}$		
			1	2	3
Raman		1,329	1,327	1,322	1,325
		1,051	1,062	1,049	1,083
		950	924	914	914
		496	486	489	489
		488	478	475	480
		364	359	362	389
		343	341	343	334
			338	339	352
		140	131	121	130
			142	142	143

s strong, *m* medium

obtained by oxidising the stable $[\text{Bu}_4\text{N}]_2[\text{Ni}(\text{dmit})_2]$ complex with iodine in methylene chloride solution. In fact, while the dianionic form of the complex does not absorb in the NIR region, the addition of iodine readily causes its oxidation to the monoanionic form, which shows a single well-defined NIR-band, with the maximum falling at 1,150 nm. The further addition of iodine causes the oxidation of the monoanion to the neutral form, which is reflected in a clearly identifiable shoulder at lower wavelengths (Fig. 6). Although the instability of the neutral species prevents to record its NIR spectrum, it is possible to decompose the spectrum obtained when both the neutral and the monoreduced forms are simultaneously present in solution. A decomposition adopting Gaussian line-shapes clearly shows that the spectrum of $[\text{Ni}(\text{dmit})_2]$ is due to a Gaussian band falling at 1,150 nm, and to a smaller one at 1,335 nm, while the neutral form shows an absorption which is due to a band at 1,001 nm with a satellite one at 860 nm. The sum of the bands of each species allows to obtain the spectral shapes of the two species, and to evaluate the maximum in the NIR absorption of the neutral species at 1,002 nm (Fig. 6). We give an estimation of the rest of the spectrum by performing a TD-DFT calculation of the excitation energies over the frequency range of interest. We make use of different approximations to the xc functional needed in the scalar relativistic ZORA Hamiltonian. To analyse the results obtained with the different approximations, we refer to the agreement found between experimental and theoretical spectra of the $[\text{Ni}(\text{H}_2\text{tmidt})_2]$ complex. All calculations have been performed on the geome-

tries optimised at ZORA level. Results obtained using the SAOP, LB94 and BP xc functionals have been calculated by taking into account scalar relativistic effects within ZORA. However, relativistic effects are not so relevant for the Ni complexes. In fact, the relativistic Ni–S bond length contraction found for the complexes **1** and **1'** [26] is about 0.010 Å. Besides, as found, the transitions mainly responsible for the calculated electronic spectra have a strong intra-ligand character, thus the relative excitation energies and oscillator strengths are only marginally affected by relativistic effects (changes on the second decimal digit for both). In line with these findings, the B3LYP and PBE0 results, calculated by Gaussian98 program, have been obtained by using an all-electron 6-31 g* basis set instead of using relativistic corrected ECPs. We first compare the various calculated spectra of the $[\text{Ni}(\text{H}_2\text{tmidt})_2]$ model complex in Table 3. All the used functionals indicate that the $[\text{Ni}(\text{H}_2\text{tmidt})_2]$ HOMO and LUMO are the $5b_{1u}$ and $5b_{2g}$ MOs, respectively. The SAOP results indicate the $6B_{3u}$ and $7B_{3u}$ excited states as mainly responsible for the absorption at 250 nm in the experimental spectrum of $[\text{Ni}(\text{Et}_2\text{tmidt})_2]$. The same assignment is found by using the BP functional, whereas the calculations with the LB94 potential indicate the $8B_{3u}$ state as responsible for the absorption. Since the corresponding excitation energies are still much lower than the ionisation threshold calculated in the SAOP functional, and the virtual orbitals mainly involved in the composition of the mentioned excited states do not sample the long-range part of the potential, the different assignment could be due to the known LB94 underestima-

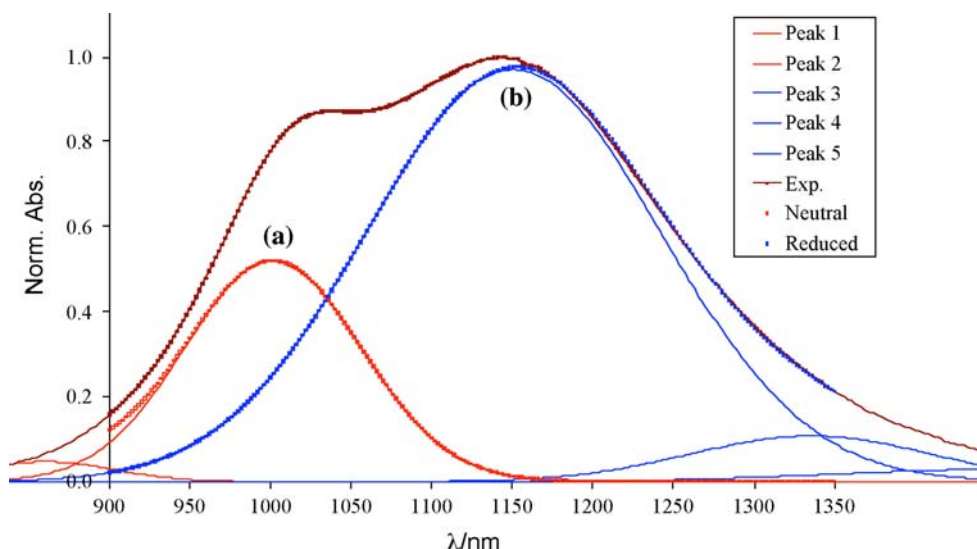


Fig. 6 Experimental (*brown line*) NIR spectrum of $[\text{Bu}_4\text{N}]_2[\text{Ni}(\text{dmit})_2]$ partially oxidised with molecular iodine and decomposition in the Gaussian bands. The sums of bands

attributed to the neutral (bands 1–2: *red line*) and monoreduced (band 3–5: *blue line*) forms allow to rebuild the spectral shapes of the two forms [(a) and (b), respectively]

Table 3 Excitation energies (eV) and composition of the most important dipole-allowed B_{2u} and B_{3u} excited states calculated for the $[\text{Ni}(\text{H}_2\text{tmidt})_2]$ model complex by using the SAOP, LB94, BP, B3LYP and PBE0 exchange-correlation functionals

State	B3LYP	PBE0	BP	LB94	SAOP
1 B_{3u}	1.52 0.2268 $5b_{1u} \rightarrow 5b_{2g}$ 0.0218 $7b_{2u} \rightarrow 8b_{1g}$	1.53 0.2315 $5b_{1u} \rightarrow 5b_{2g}$ 0.0206 $7b_{2u} \rightarrow 8b_{1g}$	1.45 90% $5b_{1u} \rightarrow 5b_{2g}$	1.31 76% $5b_{1u} \rightarrow 5b_{2g}$ 21% $8b_{2u} \rightarrow 8b_{1g}$	1.44 92% $5b_{1u} \rightarrow 5b_{2g}$ 5% $8b_{2u} \rightarrow 8b_{1g}$
2 B_{3u}	2.99 0.4169 $4b_{1u} \rightarrow 5b_{2g}$ 0.0191 $5b_{1u} \rightarrow 5b_{2g}$ 0.0176 $7b_{2u} \rightarrow 8b_{1g}$	3.10 0.4230 $4b_{1u} \rightarrow 5b_{2g}$ 0.0168 $5b_{1u} \rightarrow 5b_{2g}$ 0.0153 $7b_{2u} \rightarrow 8b_{1g}$	2.00 91% $8b_{2u} \rightarrow 8b_{1g}$	1.73 78% $8b_{2u} \rightarrow 8b_{1g}$ 19% $5b_{1u} \rightarrow 5b_{2g}$	2.08 93% $8b_{2u} \rightarrow 8b_{1g}$ 5% $5b_{1u} \rightarrow 5b_{2g}$
3 B_{3u}	3.44 0.4900 $8b_{2u} \rightarrow 8b_{1g}$	3.86 0.4917 $8b_{2u} \rightarrow 8b_{1g}$	2.70 89% $4b_{1u} \rightarrow 5b_{2g}$	2.47 86% $4b_{1u} \rightarrow 5b_{2g}$ 7% $5b_{1u} \rightarrow 6b_{2g}$	2.65 89% $4b_{1u} \rightarrow 5b_{2g}$ 6% $5b_{1u} \rightarrow 6b_{2g}$ 4% $7b_{2u} \rightarrow 8b_{1g}$
4 B_{3u}	4.49 0.3962 $5b_{1u} \rightarrow 6b_{2g}$ 0.0465 $7b_{2u} \rightarrow 8b_{1g}$	4.65 0.4005 $5b_{1u} \rightarrow 6b_{2g}$ 0.0416 $7b_{2u} \rightarrow 8b_{1g}$	3.75 78% $5b_{1u} \rightarrow 6b_{2g}$ 12% $4b_{2g} \rightarrow 6b_{1u}$	3.41 78% $5b_{1u} \rightarrow 6b_{2g}$ 9% $7b_{2u} \rightarrow 7b_{2g}$ 9% $4b_{2g} \rightarrow 6b_{1u}$	3.76 80% $5b_{1u} \rightarrow 6b_{2g}$ 9% $7b_{2u} \rightarrow 8b_{1g}$ 6% $4b_{2g} \rightarrow 6b_{1u}$
5 B_{3u}	5.00 0.2851 $7b_{2u} \rightarrow 8b_{1g}$ 0.0688 $3b_{1u} \rightarrow 5b_{2g}$ 0.0393 $5b_{1u} \rightarrow 6b_{2g}$ 0.0334 $4b_{2g} \rightarrow 6b_{1u}$	5.20 0.2951 $7b_{2u} \rightarrow 8b_{1g}$ 0.0774 $3b_{1u} \rightarrow 5b_{2g}$ 0.0382 $5b_{1u} \rightarrow 6b_{2g}$ 0.0200 $4b_{2g} \rightarrow 6b_{1u}$	4.21 67% $7b_{2u} \rightarrow 8b_{1g}$ 21% $4b_{2g} \rightarrow 6b_{1u}$ 5% $3b_{1u} \rightarrow 5b_{2g}$	3.90 66% $7b_{2u} \rightarrow 8b_{1g}$ 19% $4b_{2u} \rightarrow 6b_{1u}$ 4% $4b_{1u} \rightarrow 5b_{2g}$	4.21 71% $7b_{2u} \rightarrow 8b_{1g}$ 12% $4b_{2g} \rightarrow 6b_{1u}$ 5% $3b_{1u} \rightarrow 5b_{2g}$ 3% $4b_{1u} \rightarrow 5b_{2g}$ 3% $5b_{1u} \rightarrow 6b_{2g}$
6 B_{3u}	5.39 0.3338 $3b_{1u} \rightarrow 5b_{2g}$ 0.0750 $7b_{2u} \rightarrow 8b_{1g}$ 0.0323 $4b_{2g} \rightarrow 6b_{1u}$	5.54 0.3511 $3b_{1u} \rightarrow 5b_{2g}$ 0.0798 $7b_{2u} \rightarrow 8b_{1g}$ 0.0145 $2b_{2g} \rightarrow 6b_{1u}$	4.59 59% $2b_{2g} \rightarrow 6b_{1u}$ 12% $7b_{2u} \rightarrow 8b_{1g}$ 12% $5b_{1u} \rightarrow 6b_{2g}$ 5% $4b_{1u} \rightarrow 6b_{2g}$	4.33 56% $4b_{2g} \rightarrow 6b_{1u}$ 18% $4b_{1u} \rightarrow 6b_{2g}$ 10% $7b_{2u} \rightarrow 8b_{1g}$ 8% $5b_{1u} \rightarrow 6b_{2g}$	4.71 64% $2b_{2g} \rightarrow 6b_{1u}$ 10% $5b_{1u} \rightarrow 6b_{2g}$ 8% $7b_{2u} \rightarrow 8b_{1g}$ 6% $4b_{1u} \rightarrow 6b_{2g}$ 6% $4b_{1u} \rightarrow 5b_{2g}$
7 B_{3u}	5.58 0.3880 $2b_{2g} \rightarrow 6b_{1u}$ 0.0408 $3b_{1u} \rightarrow 5b_{2g}$ 0.0131 $3b_{3g} \rightarrow 3a_u$	5.85 0.4062 $2b_{2g} \rightarrow 6b_{1u}$ 0.0196 $3b_{1u} \rightarrow 5b_{2g}$ 0.0107 $3b_{3g} \rightarrow 3a_u$	4.86 48% $3b_{3g} \rightarrow 3a_u$ 46% $3b_{1u} \rightarrow 5b_{2g}$	4.69 66% $3b_{1u} \rightarrow 5b_{2g}$ 19% $3b_{3g} \rightarrow 3a_u$ 10% $4b_{1u} \rightarrow 6b_{2g}$	4.86 76% $3b_{1u} \rightarrow 5b_{2g}$ 9% $4b_{1u} \rightarrow 6b_{2g}$ 5% $3b_{3g} \rightarrow 3a_u$
8 B_{3u}	6.19 0.4266 $3b_{3g} \rightarrow 3a_u$ 0.0326 $4b_{1u} \rightarrow 6b_{2g}$ 0.0118 $3b_{2g} \rightarrow 6b_{1u}$	6.51 0.3751 $3b_{3g} \rightarrow 3a_u$ 0.0531 $4b_{1u} \rightarrow 6b_{2g}$ 0.0186 $3b_{2g} \rightarrow 6b_{1u}$ 0.0147 $2a_u \rightarrow 4b_{3g}$ 0.0137 $2b_{2g} \rightarrow 6b_{1u}$	5.02 44% $3b_{3g} \rightarrow 3a_u$ 38% $3b_{1u} \rightarrow 5b_{2g}$ 8% $2a_u \rightarrow 4b_{3g}$	4.85 54% $3b_{3g} \rightarrow 3a_u$ 26% $4b_{1u} \rightarrow 6b_{2g}$ 8% $3b_{2g} \rightarrow 6b_{1u}$	5.31 41% $4b_{1u} \rightarrow 6b_{2g}$ 34% $3b_{3g} \rightarrow 3a_u$ 18% $3b_{2g} \rightarrow 6b_{1u}$
4 B_{3u}	5.33 0.3307 $1a_u \rightarrow 5b_{2g}$ 0.0668 $9b_{3u} \rightarrow 8b_{1g}$ 0.0261 $3b_{3g} \rightarrow 6b_{1u}$ 0.0174 $5b_{1u} \rightarrow 4b_{3g}$	5.48 0.2937 $1a_u \rightarrow 5b_{2g}$ 0.1059 $9b_{3u} \rightarrow 8b_{1g}$ 0.0240 $5b_{1u} \rightarrow 4b_{3g}$	4.39 51% $5b_{1u} \rightarrow 4b_{3g}$ 29% $10b_{3u} \rightarrow 8b_{1g}$ 6% $1a_u \rightarrow 5b_{2g}$ 3% $4b_{1u} \rightarrow 4b_{3g}$	4.15 63% $5b_{1u} \rightarrow 4b_{3g}$ 19% $10b_{3u} \rightarrow 8b_{1g}$ 5% $4b_{1u} \rightarrow 4b_{3g}$ 4% $2a_u \rightarrow 5b_{2g}$	4.44 45% $5b_{1u} \rightarrow 4b_{3g}$ 28% $3b_{3g} \rightarrow 6b_{1u}$ 14% $10b_{3u} \rightarrow 8b_{1g}$ 4% $1a_u \rightarrow 5b_{2g}$

In the B3LYP and PBE0 excited state compositions, the relative weights of the linearly combined singly excited Slater determinants are represented by the normalised squared coefficients of the linear combination

tion of the excitation energies. The remaining SAOP excitation energies are similar to those calculated by using the BP and LB94 functionals. In particular, the SAOP functional describes the NIR excitation energy better than the BP functional, but not better than the LB94 potential. Besides, the excitation energy to the $2B_{3u}$ excited state is larger than those calculated by the BP and LB94 functionals, thus better reproducing the experimental value, though yet underestimated as becomes clear from Fig. 7. We have also used other two functionals for our calculations, both implemented

in the Gaussian98 package: B3LYP and PBE0. The PBE0 model gives results closer to those calculated by using the B3LYP functional (Fig. 7). Both give the worse results for the NIR absorption and the absorption ranging between 250 and 350 nm. On the other hand, both the functionals swap the composition of the $2B_{3u}$ and $3B_{3u}$ with respect to that calculated by the others. Thus, the excitation energy to the $3B_{3u}$ is very well described by these two hybrid functionals, whereas that of the $2B_{3u}$ is overestimated with respect to those calculated by the pure ones, even if it is much more

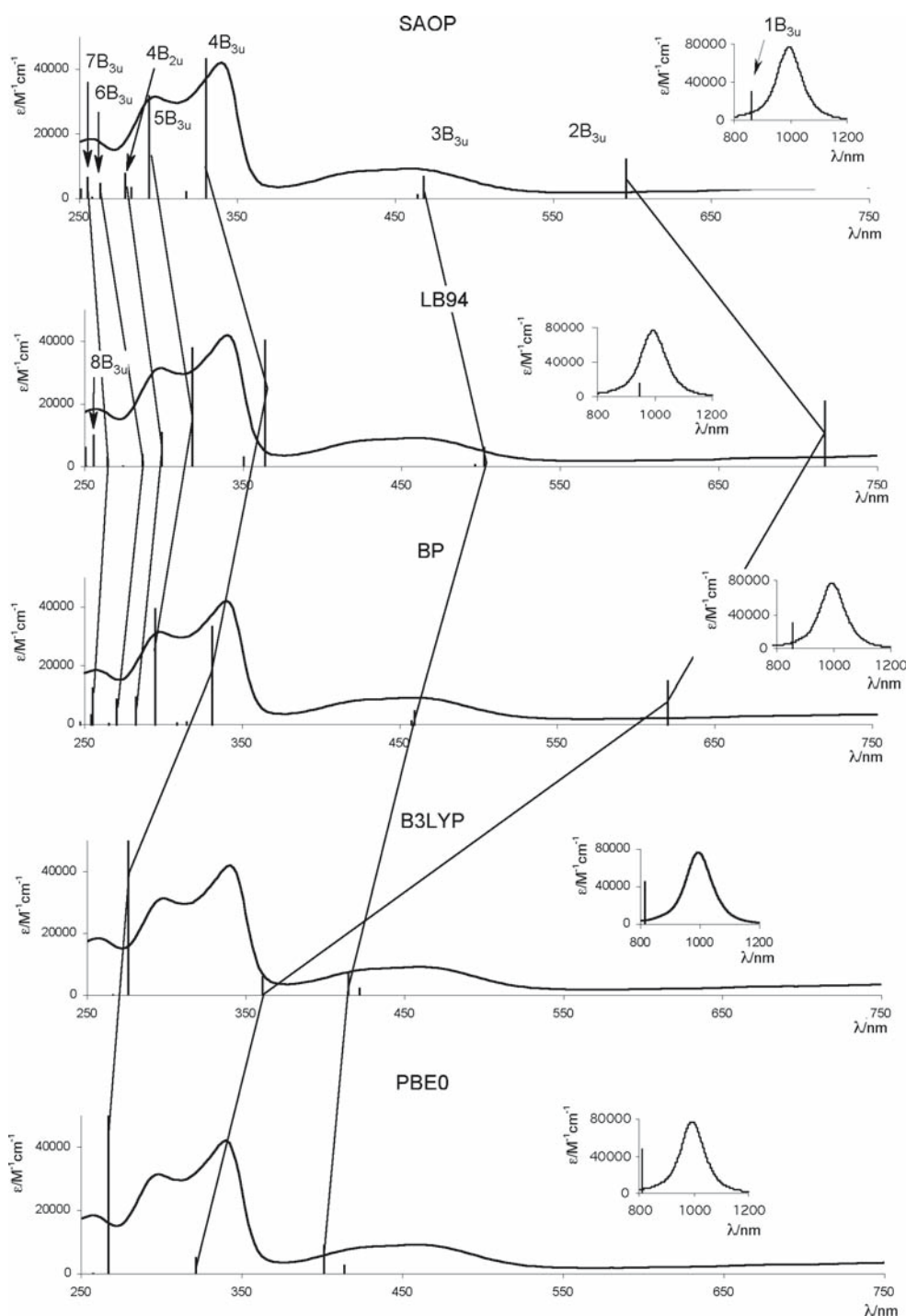


Fig. 7 Experimental UV-vis-NIR spectrum of $[\text{Ni}(\text{Et}_2\text{timdt})_2]$ recorded in CHCl_3 solution. The most important singlet-singlet excitation energies (oscillator strengths $>10^{-3}$) calculated for the $[\text{Ni}(\text{H}_2\text{timdt})_2]$ model complex by using different xc-functionals

(SAOP, LB94, BP, B3LYP and PBE0) in a TD-DFT framework are reported. The insets contain the excited state responsible for the absorption in the NIR region, which is calculated to be the 1^1B_{3u} by all the used functionals

close to the experimental value. On the basis of these results, the spectrum of the $[\text{Ni}(\text{dmit})_2]$ complex has been calculated using three different xc-functionals: SAOP, LB94 and B3LYP (Fig. 8). We have reported the excitations energies and the compositions of the various

calculated excited states in Table 4. Also for this complex, the B3LYP gives a different order of the excited states with respect to the order found by the other two functionals. In particular, the states 2B_{3u} , 3B_{3u} and 4B_{3u} calculated by the B3LYP show a composition sim-

ilar to that of the $3B_{3u}4B_{3u}$ and $2B_{3u}$, respectively, calculated by the SAOP and LB94. On the other hand, the remaining states show a similar composition. Excellent results obtained for the $[\text{Ni}(\text{H}_2\text{timdt})_2]$ complex by using the SAOP and LB94 suggest that also for the $[\text{Ni}(\text{dmit})_2]$ complex these two functionals may accurately describe its spectrum. The composition of the excited states $1B_{3u} - 4B_{3u}$ is similar to that found for the $[\text{Ni}(\text{H}_2\text{timdt})_2]$ complex, whereas the two complexes are quite different in the spectral region ranging between 250 and 400 nm. In fact, for the $[\text{Ni}(\text{dmit})_2]$ much more states are responsible for the absorption in this region. In particular, both the SAOP and LB94 functionals indicate the excited states $5B_{3u} - 7B_{3u}$, together with the $8B_{2u}$, as those mainly involved in the absorption. Besides, other transitions show a large oscillator strength, though they are not the same in the SAOP and LB94 calculations: the transitions to the $8 - 10B_{3u}$ states by using the former, and to the $8 - 12B_{3u}$, together with that to the $13B_{2u}$ one, by using the latter. It is noteworthy that the excited state $9B_{3u}$ calculated by the SAOP shows a composition similar to that of the state $8B_{3u}$ calculated by the LB94 potential. As shown in Table 4, the compositions of the states $5B_{3u}$ and $7B_{3u}$ are similar to those of the states $6B_{3u}$ and $5B_{3u}$, respectively, calculated for the $[\text{Ni}(\text{H}_2\text{timdt})_2]$ complex. On the other hand, the states $6B_{3u}$ and $8B_{2u}$ show a very different composition. In particular, the state $6B_{3u}$ has a strong intra-ligand character, with a small ligand-to-metal-charge-transfer (LMCT) contribution by the $7B_{2u} \rightarrow 8b_{1g}$ one-electron transition, and the state $8B_{2u}$ has a strong, even though not predominant, LMCT character, missing in the case of the $[\text{Ni}(\text{H}_2\text{timdt})_2]$ complex. Besides, the states $9B_{3u}$ (main component: $8b_{2g} \rightarrow 6b_{1u}$) and $10B_{3u}$ (main component: $12a_g \rightarrow 11b_{3u}$) calculated by the LB94 potential show a very strong metal-to-ligand-charge-transfer (MLCT) character. A very interesting result is observed for the NIR excitation energy. Both the LB94 and SAOP functionals indicate a bathochromic shift for the $[\text{Ni}(\text{dmit})_2]$ complex with respect to the $[\text{Ni}(\text{H}_2\text{timdt})_2]$ one. The calculations by using the B3LYP are not useful in this case because they give same excitation energy for the two complexes (1.5271 and 1.5213 eV for **1** and **1'**, respectively). Since for the $[\text{Ni}(\text{H}_2\text{timdt})_2]$ complex the LB94 potential overestimates the NIR experimental excitation energy by 0.06 eV, the same might be expected in the case of the $[\text{Ni}(\text{dmit})_2]$. Thus, we suggest that the NIR absorption for this complex is located very close to the estimation found experimentally at 1,002 nm. This is a very important result for possible applications as dyes for Q-switching and/or mode locking the Nd:YAG (1,064 nm) and Nd:YLF (1,053 nm) lasers.

4 Conclusions

We have systematically studied the structural, electronic and optical properties of the $[\text{M}(\text{dmit})_2]$ ($\text{M} = \text{Ni}$, **1**; Pd , **2**; Pt , **3**) neutral dithiolenes within a density functional approach in combination with the ZORA method to treat the dominant scalar relativistic effects. We have compared their properties with those of the previously studied $[\text{M}(\text{H}_2\text{timdt})_2]$ ($\text{M} = \text{Ni}$, **1'**; Pd , **2'**; Pt , **3'**) model complexes. The $[\text{M}(\text{dmit})_2]$ complexes show shorter M–S bond distances, weaker M–ligand bonding energies and larger HOMO–LUMO energy gaps with respect to the corresponding $[\text{M}(\text{H}_2\text{timdt})_2]$ metal-dithiolenes. We found that the LUMOs in the $[\text{M}(\text{dmit})_2]$ compounds have energies more negative than those in the corresponding $[\text{M}(\text{H}_2\text{timdt})_2]$ compounds, in line with the experimental finding that the former are more reducible than the latter and that their anionic forms are more stable than the neutral ones. Furthermore, a very intriguing finding is the quasi-degeneracy of the corresponding $[\text{M}(\text{dmit})_2]$ LUMOs and $[\text{M}(\text{H}_2\text{timdt})_2]$ HOMOs, which may candidate the mixed-ligand complexes as promising non-linear optical materials. The vibrational spectrum has been calculated for the $[\text{M}(\text{dmit})_2]$ series and the assignment of the experimental $[\text{Ni}(\text{dmit})_2]$ spectrum has been performed. Our results show some differences with respect to previous assignments, in particular for the Raman band at 496 cm^{-1} and for the two FIR bands at 485 and 328 cm^{-1} . Results calculated for the vibrational spectrum of the compounds **2** and **3**, for which no experimental data are available, show another medium intensive FIR band at 484 and 362 cm^{-1} , respectively, too weak in the $[\text{Ni}(\text{dmit})_2]$ spectrum to be observed. Furthermore, the comparison between the $[\text{Ni}(\text{H}_2\text{timdt})_2]$ and $[\text{Ni}(\text{dmit})_2]$ vibrational spectra in the spectral region $50\text{--}500\text{ cm}^{-1}$, reveals that the nature of the lowest frequency Raman and FIR bands is different for the two complexes. New excitation energy calculations on the compound **1'** by using different xc functionals (B3LYP, PBE0, BP, LB94, SAOP) have indicated the functionals better describing the different region of the $[\text{Ni}(\text{H}_2\text{timdt})_2]$ spectrum, so that the optical spectrum of the $[\text{Ni}(\text{dmit})_2]$ complex has been calculated by using the LB94, SAOP and B3LYP functionals. An important feature for possible applications of the studied complexes in the non-linear optical field is the position of the NIR absorption, which falls around 1,000 nm for the complex **1**, thus showing a bathochromic shift with respect to the complex **1'**. Other differences between the spectra of the two complexes are found in the spectral region 250–400 nm. Indeed a larger number of excited states are responsible for the absorption in this frequency range in the case of

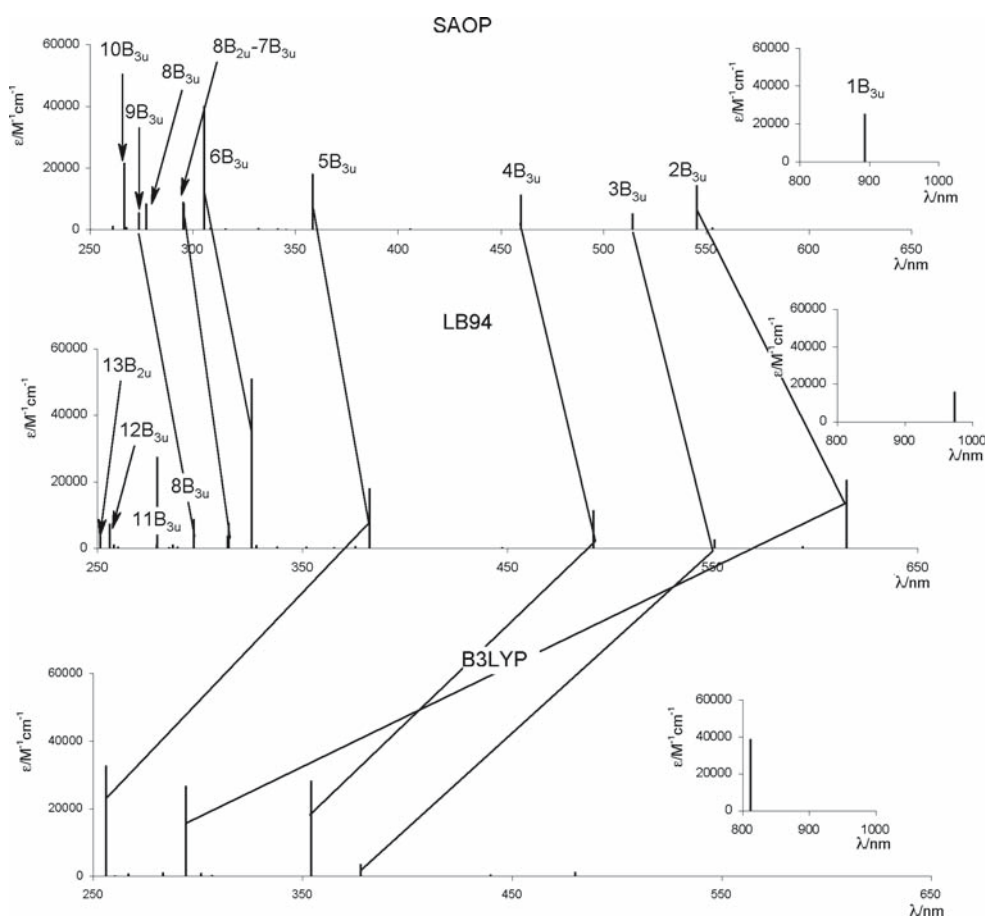


Fig. 8 The most important singlet-singlet excitation energies (oscillator strengths $>10^{-3}$) calculated for the $[\text{Ni}(\text{dmit})_2]$ complex by using different xc-functionals (SAOP, LB94 and B3LYP)

in a TD-DFT framework are reported. The insets contain the excited states responsible for the absorption in the NIR region, which is calculated to be the 1^1B_{3u} by all the used functionals

Table 4 Excitation energies (eV) and composition of the most important dipole-allowed B_{2u} and B_{3u} excited states calculated for the $[\text{Ni}(\text{dmit})_2]$ complex by using the SAOP, LB94 and B3LYP exchange-correlation functionals

State	B3LYP	LB94	SAOP
1 B_{3u}	1.53 0.2747 $5b_{1u} \rightarrow 5b_{2g}$ 0.0227 $7b_{2u} \rightarrow 8b_{1g}$	1.28 86% $5b_{1u} \rightarrow 5b_{2g}$ 11% $8b_{2u} \rightarrow 8b_{1g}$	1.39 91% $5b_{1u} \rightarrow 5b_{2g}$ 5% $8b_{2u} \rightarrow 8b_{1g}$
2 B_{3u}	2.82 0.4056 $4b_{1u} \rightarrow 5b_{2g}$ 0.0439 $5b_{1u} \rightarrow 6b_{2g}$ 0.0204 $7b_{2u} \rightarrow 8b_{1g}$	2.02 80% $8b_{2u} \rightarrow 8b_{1g}$ 8% $5b_{1u} \rightarrow 5b_{2g}$	2.27 80% $8b_{2u} \rightarrow 8b_{1g}$ 12% $5b_{1u} \rightarrow 6b_{2g}$ 4% $4b_{1u} \rightarrow 5b_{2g}$
3 B_{3u}	3.28 0.3245 $5b_{1u} \rightarrow 6b_{2g}$ 0.1032 $8b_{2u} \rightarrow 8b_{1g}$ 0.0200 $4b_{1u} \rightarrow 5b_{2g}$ 0.0111 $7b_{2u} \rightarrow 8b_{1g}$	2.26 60% $4b_{1u} \rightarrow 5b_{2g}$ 28% $5b_{1u} \rightarrow 6b_{2g}$	2.41 60% $4b_{1u} \rightarrow 5b_{2g}$ 22% $5b_{1u} \rightarrow 6b_{2g}$ 9% $8b_{2u} \rightarrow 8b_{1g}$ 4% $7b_{2u} \rightarrow 8b_{1g}$ 3% $5b_{1u} \rightarrow 5b_{2g}$
4 B_{3u}	3.50 0.3705 $8b_{2u} \rightarrow 8b_{1g}$ 0.0815 $5b_{1u} \rightarrow 6b_{2g}$ 0.0158 $2b_{2g} \rightarrow 6b_{1u}$	2.52 51% $5b_{1u} \rightarrow 6b_{2g}$ 26% $4b_{1u} \rightarrow 5b_{2g}$ 16% $2b_{2g} \rightarrow 6b_{1u}$	2.70 55% $5b_{1u} \rightarrow 6b_{2g}$ 25% $4b_{1u} \rightarrow 5b_{2g}$ 14% $2b_{2g} \rightarrow 6b_{1u}$ 3% $8b_{2u} \rightarrow 8b_{1g}$
5 B_{3u}	4.21 0.4228 $2b_{2g} \rightarrow 6b_{1u}$ 0.0112 $7b_{2u} \rightarrow 8b_{1g}$	3.24 63% $2b_{2g} \rightarrow 6b_{1u}$ 24% $4b_{1u} \rightarrow 6b_{2g}$ 6% $5b_{1u} \rightarrow 6b_{2g}$	3.46 68% $2b_{2g} \rightarrow 6b_{1u}$ 19% $4b_{1u} \rightarrow 6b_{2g}$ 6% $5b_{1u} \rightarrow 6b_{2g}$

Table 4 continued

State	B3LYP	LB94	SAOP
6 B _{3u}	4.84 0.2723 7b _{2u} → 8b _{1g} 0.0970 3b _{1u} → 5b _{2g} 0.0416 4b _{1u} → 6b _{2g}	3.82 39% 4b _{1u} → 6b _{2g} 39% 7b _{2u} → 8b _{1g} 6% 3b _{1u} → 5b _{2g} 4% 3b _{2g} → 6b _{1u}	4.06 46% 4b _{1u} → 6b _{2g} 28% 7b _{2u} → 8b _{1g} 10% 3b _{1u} → 5b _{2g} 7% 3b _{2g} → 6b _{1u}
7 B _{3u}	5.05 0.3567 4b _{1u} → 6b _{2g} 0.0541 7b _{2u} → 8b _{1g} 0.0135 3b _{1u} → 5b _{2g}	3.96 36% 7b _{2u} → 8b _{1g} 20% 3b _{2g} → 6b _{1u} 20% 4b _{1u} → 6b _{2g} 8% 2b _{2g} → 6b _{1u} 5% 4b _{1u} → 5b _{2g}	4.19 45% 7b _{2u} → 8b _{1g} 23% 3b _{2g} → 6b _{1u} 14% 4b _{1u} → 6b _{2g} 5% 2b _{2g} → 6b _{1u} 4% 4b _{1u} → 5b _{2g}
8 B _{3u}	5.19 0.2950 3b _{1u} → 5b _{2g} 0.0579 3b _{3g} → 3a _u 0.0549 7b _{2u} → 8b _{1g} 0.0288 4b _{1u} → 6b _{2g} 0.0240 2a _u → 4b _{3g}	4.18 84% 3b _{3g} → 3a _u 12% 2a _u → 4b _{3g} 3% 3b _{1u} → 5b _{2g}	4.47 39% 3b _{1u} → 5b _{2g} 23% 3b _{3g} → 3a _u 22% 3b _{2g} → 6b _{1u} 10% 7b _{2u} → 8b _{1g}
9 B _{3u}	– ^a	4.29 63% 3b _{2g} → 6b _{1u} 15% 3b _{1u} → 5b _{2g} 7% 4b _{1u} → 6b _{2g} 4% 7b _{2u} → 8b _{1g} 3% 2b _{2g} → 6b _{1u}	4.53 56% 3b _{3g} → 3a _u 27% 3b _{2g} → 6b _{1u} 9% 2a _u → 4b _{3g} 4% 6b _{1u} → 6b _{2g}
10 B _{3u}	–	4.35 96% 12a _g → 11b _{3u}	4.65 36% 2a _u → 4b _{3g} 28% 3b _{1u} → 5b _{2g} 18% 3b _{2g} → 6b _{1u} 7% 4b _{1u} → 6b _{2g} 3% 7b _{1g} → 9b _{3u} 3% 2b _{2g} → 6b _{1u}
11 B _{3u}	–	4.45 44% 2a _u → 4b _{3g} 41% 3b _{1u} → 5b _{2g} 5% 3b _{2g} → 6b _{1u}	– ^a
12 B _{3u}	–	4.86 31% 10b _{3u} → 13a _g 27% 2a _u → 4b _{3g} 22% 3b _{1u} → 5b _{2g} 8% 3b _{3g} → 3a _u	–
8 B _{2u}	5.36 0.2656 7b _{1g} → 11b _{3u} 0.2327 8b _{2u} → 13a _g	3.95 27% 10b _{3u} → 8b _{1g} 22% 1a _u → 5b _{2g} 21% 5b _{1u} → 4b _{3g} 8% 4b _{1u} → 4b _{3g} 6% 7b _{1g} → 11b _{3u} 4% 2b _{3g} → 6b _{1u} 3% 2a _u → 5b _{2g}	4.20 43% 10b _{3u} → 8b _{1g} 18% 5b _{1u} → 4b _{3g} 15% 1a _u → 5b _{2g} 7% 3b _{1u} → 4b _{3g} 3% 7b _{1g} → 11b _{3u} 3% 2a _u → 5b _{2g} 3% 2b _{3g} → 6b _{1u}
13 B _{2u}	–	4.97 55% 4b _{1u} → 4b _{3g} 24% 8b _{2u} → 14a _g 5% 3b _{2g} → 3a _u 4% 7b _{2u} → 13a _g	–

In the B3LYP excited state compositions, the relative weights of the linearly combined singly excited Slater determinants are represented by the normalised squared coefficients of the linear combination

^a The missing B3LYP and SAOP excitation energies are much higher than the LB94 ones and they have not been computed being not relevant in describing the spectrum in the experimental frequency window

complex **1**. On the other hand, the spectrum, in particular in this spectral region, has still a predominant intra-ligand character, as found for compound **1'**.

Acknowledgments LASCAMM (Laboratorio per la Sintesi e la Caratterizzazione dei Materiali Molecolari) through grants within “P.O. 5 Cluster 14”, from MIUR Cofin2000 and FISIR1999 are gratefully acknowledged for financial support. Dr. Carla Denotti is gratefully acknowledged for recording UV–vis–NIR spectra.

References

- Aragoni MC, Arca M, Demartin F, Devillanova FA, Garau A, Isaia F, Lelj F, Lippolis V, Verani G (1999) *J Am Chem Soc* 121:7098
- Nakamura T, Underhill AE, Coomber AT, Friend RH, Tajima H, Kobayashi A, Kobayashi H (1995) *Inorg Chem* 34:870
- Williams R, Billing E, Waters JH, Gray HB (1966) *J Am Chem Soc* 88:43
- Ferraro JR, Williams JM (1987) *Introduction to synthetic electrical conductors*. Academic, New York
- Cassoux P, Valade L, Kobayashi H, Kobayashi A, Clark RA, Underhill AE (1991) *Coord Chem Rev* 110:115
- Pomaréde B, Garreau B, Malfant I, Valade L, Cassoux P, Legros JP, Audouard A, Brossard L, Ulmet JP, Doublet ML, Canadell E (1994) *Inorg Chem* 33:3401
- Sun S, Wu P, Zhu D, Ma Z, Shi N (1998) *Inorg Chim Acta* 268:103
- Sato A, Kobayashi H, Naito T, Sakai F, Kobayashi A (1997) *Inorg Chem* 36:5262
- Kochurani, Singh HB, Jasisinski JP, Paight ES, Butcher RJ (1997) *Polyhedron* 16:3505
- Matsubayashi G, Natsuaki K, Nakano M, Tamura H, Arakow R (1997) *Inorg Chim Acta* 262:103
- Yeldhuizen Y, Veldman N, Lakin MT, Spek AL, Paulus PM, Faulmann C, Haasnoot JG, Maaskant MJA, Reedijk J (1996) *Inorg Chim Acta* 245:27
- Fujiwara H, Arai E, Kobayashi H (1997) *J Chem Soc Chem Commun* 9:837
- Faulman C, Cassoux C (2004) *Prog Inorg Chem* 52:399
- Cummings SD, Eisenberg R (2004) *Prog Inorg Chem* 52:315
- McMaster J, Tunnel JM, Garner CD (2004) *Prog Inorg Chem* 52:539
- Kirk ML, McNaughton RL, Helton ME (2004) *Prog Inorg Chem* 52:111
- Kato R (2004) *Chem Rev* 104:5319
- Hohenberg P, Kohn W (1964) *Phys. Rev. B* 136:864
- Casida ME (1995) Chong DP (ed) *Recent advances in Density Functional Methods, Part I*. World Scientific, Singapore, p 155
- Casida ME (1996) Seminario JM (ed) *Recent developments and applications of modern density functional theory*. Elsevier, Amsterdam, p 391
- Pyykkö P (1988) *Chem Rev* 88:563
- Pyykkö P (1991) Wolson S, Grant IP and Gyorffy BL (eds) *The effect of relativity in atom, molecules and solid-state*. Plenum, New York, p 1
- van Lenthe E (1996) PhD thesis, Free University, Amsterdam
- van Lenthe E, Baerends EJ, Snijders JG (1993) *J Chem Phys* 99:4597
- van Lenthe E, Baerends EJ, Snijders JG (1994) *J Chem Phys* 101:9783
- Romaniello P, Aragoni MC, Arca M, Cassano T, Denotti C, Devillanova FA, Isaia F, Lelj F, Lippolis V, Tommasi R (2003) *J Phys Chem A* 107:9679
- Romaniello P, Lelj F (2003) *Chem Phys Lett* 372:51
- Romaniello P, Lelj F (2003) *J Mol Struct Theochem* 636:23
- Cassano T, Tommasi R, Nitti L, Aragoni MC, Arca M, Denotti C, Devillanova FA, Isaia F, Lippolis V, Lelj, Romaniello P (2003) *J Chem Phys* 118:5995
- van Gisbergen SJA (1998) PhD thesis, Free University, Amsterdam
- Rosa A, Ricciardi G, Gritsenko OV, Baerends EJ (2004) *Struct Bonding* 112:49 (For a recent overview of the performance of the various GGA and hybrid functionals on transition metal complexes)
- Becke A (1988) *Phy Rev A* 38:3098
- Perdew JP (1986) *Phys Rev B* 33:8822
- Lee C, Yang W, Parr RG (1988) *Phys Rev B* 37:785
- Becke AD (1993) *J Chem Phys* 98:5648
- Perdew JP, Burke K, Ernzerhof M (1997) *Phys Rev Lett* 77:3865
- Adamo C, Barone V (1999) *J Chem Phys* 110:6158
- van Leeuwen R, Baerends EJ (1994) *Phys Rev A* 49:2421
- Davidson ER (1975) *J Comp Phys* 17:87
- van Gisbergen SJA, Groenevald JA, Rosa A, Snijders JG, Baerends EJ (1999) *J Phys Chem A* 103:6835
- Frisch MJ, Trucks GW, Schlegel HB, Scuseria GE, Robb MA, Cheeseman JR, Zakrzewski VG, Montgomery JA, Stratmann RE, Burant JC, Dapprich S, Millam JM, Daniels AD, Kudin KN, Strain MC, Farkas O, Tomasi J, Barone V, Cossi M, Cammi R, Mennucci B, Pomelli C, Adamo C, Clifford S, Ochterski J, Petersson GA, Ayala PY, Cui Q, Morokuma K, Malick DK, Rabuck AD, Raghavachari K, Foresman JB, Cioslowski J, Ortiz JV, Stefanov BB, Liu G, Liashenko A, Piskorz P, Komaromi I, Gomperts R, Martin RL, Fox DJ, Keith T, Al-Laham MA, Peng CY, Nanayakkara A, Gonzalez C, Challacombe M, Gill PMW, Johnson BG, Chen W, Wong MW, Andres JL, Head-Gordon M, Replogle ES, Pople JA (1998) *Gaussian 98*, Gaussian, Inc, Pittsburgh, PA
- Fonseca Guerra C, Visser O, Snijders JG, te Velde G, Baerends EJ (1995) In: Clementi E, Corongiu G (eds) *Methods and techniques of computational chemistry*, STEF, Cagliari, p 303
- ADF STO basis sets available on line at <http://www.scm.com/Downloads/Downloads.html>
- Valde L, Legros JP, Bousseau M, Cassoux P, Garbouskas M, Interrante LV (1985) *J Chem Soc Dalton Trans* 4:783
- Arca M, Demartin F, Devillanova FA, Garau A, Isaia F, Lelj F, Lippolis V, Pedraglio S, Verani G (1998) *J Chem Soc Dalton Trans* 22:3731
- Aragoni MC, Arca M, Crisponi G, Nurchi VM (1995) *Anal Chim Acta* 316:195
- Ziegler T, Rauk A (1977) *Theor Chim Acta* 46:1
- Ziegler T, Rauk A (1979) *Inorg Chem* 18:1558
- van Gisbergen SJA, Snijders JG, Baerends EJ (1997) *Phys Rev Lett* 78:3097
- Pokhodnya KI, Faulmann C, Malfant I, Andreu-Solano R, Cassoux P, Mlayah A, Smirnov D, Leotin J (1999) *Synth Met* 103:2016
- Liu HL, Tanner DB, Pullen AE, Abboud KA, Reynolds JR (1996) *Phys Rev B* 53:10557